



Kashf Journal of Multidisciplinary Research

Vol: 02 - Issue 09 (2025)

P-ISSN: 3007-1992 E-ISSN: 3007-200X

https://kjmr.com.pk

IRON OXIDE BASED NANOCOMPOSITES AS ELECTRODE MATERIAL FOR SUPERCAPACITORS

Murtaza Abbas*

University of Okara, Punjab, Pakistan

*Corresponding Author: murtazaabbas776@gmail.com

Article Info



Abstract

Supercapacitors (SCs) are an extremely effective and environmentally friendly type of electrochemical energy storage devices that have gained a lot of attention as an alternative for batteries. The limited electrical conductivity of a supercapacitor must be greatly boosted in order to facilitate rapid charging and discharging. Among the diverse electrode materials examined, iron oxide compounds have attracted extensive investigation as promising anode constituents for supercapacitors owing to their broad operating potential range under negative bias, exceptionally high theoretical gravimetric capacity, favorable redox kinetics, natural abundance, and environmental friendliness. However, iron oxides continue to struggle with deficiencies of inadequate longevity and weak conductivity. This survey aims recapitulate recent breakthroughs involving iron oxide-derived nanostructures, such as carbon-coated iron oxides (C@Fe₂O₃) and nickel and carbon-coated iron oxide (Ni@C@Fe₂O₃) that exhibit utility as electrode components for supercapacitors. Supercapacitors show great promise for applications in portable electronics and wearable technology. Iron oxide nanomaterials can be engineered into versatile electrode composites with properties well-suited to these uses. When configured as all-solid-state or transparent, flexible assemblies, such supercapacitors leverage the wideranging capabilities of their constituent nanoscale components. Continued progress in the synthesis of multicomponent nanocomposites will likely guide future leaps toward increasingly powerful and durable energy storage solutions.



This article is an open access article distributed under the terms and conditions of the Creative Commons Attribution (CC BY) license https://creativecommon

https://creativecommon s.org/licenses/by/4.0

Keywords:

supercapacitors; iron oxides; nanomaterials; nanocomposites; energy storage; charging and discharging; stability.

1. INTRODUCTION

Ancient people made the innovation of the storage of electric charge on a surface as a result of phenomena related to amber rubbing. The effects of such occurrences were known around the middle of the eighteenth century when Static Electricity, a branch of physics, was researched and several kinds of electric gear were constructed [1]. The 1800 discovery of voltaic electricity by Volta opened the door for the creation of electrochemical energy. Following then, it underwent several changes during the 1900s. Reversible rechargeable batteries have since emerged as a significant advancement in the field of applied electrochemistry [2]. With the Becker patent, which was issued in 1957, a latest category of repairable, electrical, and analytical energy storage device was industrial. This device also make to use of a specific capacity linked to the charge-discharge of a double layer at electrode interface or a pseudo-capacitance coupled to electro-sorption or oxidation-reduction process that take place at the electrode interface. The better specific capacity of the active electrode material at the interface, whether in powdered or felted form, the larger the specific area of carbon will be [3]. When using conductive polymers with a elevated surface area or oxides, an important amount of pseudo capacitance may be produced [4].

Recent decades have seen a decline of the energy and environmental issue caused by the use of fossil fuels, foremost to enormously high governance costs. There will inevitably be an energy crisis because of the rising usage of energy equipment brought on by rapid economic and population expansion [5]. The public's interest in research on renewable energy and energy efficiency has increased as a result. Society must transition to clean and renewable energy sources while simultaneously managing resource use. But there are issues with current energy storage systems that need to be fixed. As a result, the present level of energy usage will continue for a while. To solve these problems and lessen pollution and resource loss, scientists are developing innovative materials and techniques [6-11]. The most obvious result of the previous several decades has been an increase in the production of green, clean energy from numerous sources. Many electric cars and pieces of equipment utilize this green energy. Uneven geographical distribution limits fuel use, calling for creative energy storage systems and effective energy conversion technologies. Utilizing the sporadic power generated by these renewable resources requires an effective energy storage system. Additionally, the growth of renewable and hygienic energy sources quickens as living standards rise, environmental consciousness increases, and the economy grows [12,13].

As a result of worldwide warming, environmental deterioration, and the reduction of fossil fuel supplies, effective energy sources are critically needed today (3). The conventional usage of fossil fuels for energy must be reduced to create a low-carbon economy and reduce pollution. Devices using clean and renewable energy must be developed for this purpose [14-19]. Because electricity is a clean energy source and it is frequently utilized in daily life for a variety of functions. Electric energy storage technology (like supercapacitors and secondary batteries) are in high demand as the use of consumer electric devices and electric vehicles increases. (Fig. 1.1). They require energy and power devices with superior energy and power densities and longer life spans. The most frequently used secondary batteries in the recent world are lithium-ion batteries (LIBs), nickel-metal hydride batteries, and lead-acid batteries. Abundant other batteries are also offered including Na-ion batteries (SIBs), Zinc-ion batteries (ZIBs), Li-ion batteries (LIBs), Li-S batteries (LSBs), Li-metal batteries (LMBs), Mg-ion batteries (MIBs), and electrochemical capacitors (ECs) [20-27]. Their drawbacks include their slow rate of charging, little power density, and

tiny cycle life. In the direction of a larger extent, significant work has been done to enhance their performance and develop effective electrode materials [28].



Figure 1.1: Kinds of Energy Storage Devices [18]

Performance of the energy storage devices may be described by two key variables: energy and power. Power density explains how quickly and evenly charges are dispersed, whereas energy density specifies how much a device can store charge [29-37]. The Ragone plot, shown in Fig. 1.2, is a useful tool for explaining both energy and power densities [38].

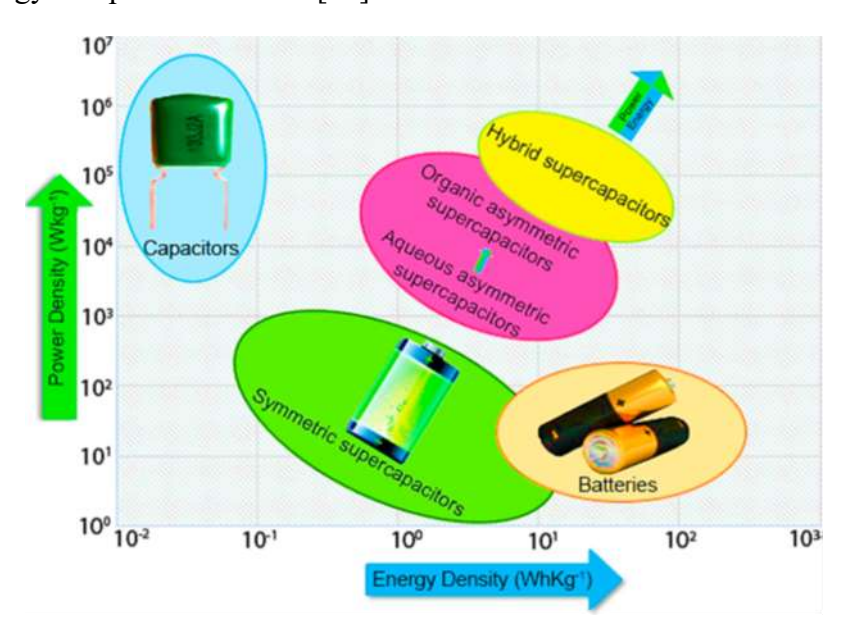


Figure 1.2: Power energy density range for different electrochemical energy storage of ragone plot [38]

When specific power is increased, i.e., when the rate of charging of a device is increased, then the stored amount of energy is decreased at the maxima point. This happens because of oxidation and reduction reactions and ion transport mechanisms. This means that changing electrical energy to charge storage is not taken a maximum time frame. As a consequence, excessive energy is lost in type of heat to the surroundings [39-47]. Fig 1.2 represents the performance of four electrochemical capacitor devices through a reparatory funnel that is being charged from basal hole. Whether every device has a similar mass, then the whole volume of the funnel is specific utmost energy (U). It is described as the maximum amount of charge which is stored in a device. The area of the opening in the stopcock is attributed to specific highest power (P) [48-55]. Specific maximum power increases rates of charge and discharge by the utmost. Comparing the performance of four devices, the first device represents the lowest power density and energy density while second device shows maximum energy and power like a super capacitor [56].

2. Materials and methods

Scheme of Research Work:

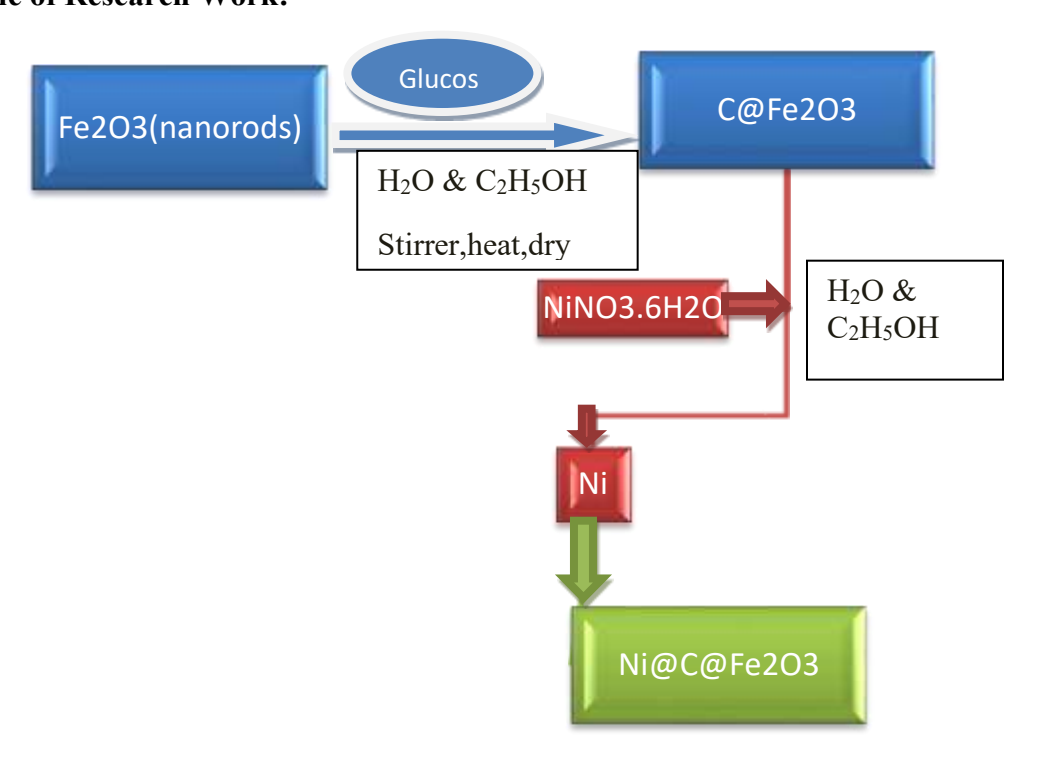


Figure 2.1: Schematic diagram of Fe₂O₃ nanorods, C@ Fe₂O₃, Ni@C@ Fe₂O₃prepared via Hydrothermal Method

2.1. Chemical Reagents:

Ferric chloride hexahydrate (FeCl₃.6H₂O) [sigma-99.9% pure], 6M Potassium Hydroxide (KOH) [sigma-99.9% pure], Water (H₂O) [distilled for two times], Urea (NH₂CONH₂) [sigma-99.9% pure], Ethanol (C₂H₅OH) [gradient grade], and Glucose (C₆H₁₂O₆) [sigma-99.9% pure]. All these chemicals were supplied by Hajvery traders Lahore (Pakistan).

2.2. Synthesis of Iron Oxide (Fe₂O₃) Nano rods:

0.5 g FeCl₃.6H₂O was added to aqueous solution containing 2 ml of 6 M KOH, 10 ml H₂O and 1 g urea with magnetic stirring for 1 h. Then this solution was taken in Teflon-lined stainless steel autoclave of 50 ml after that it was heated at 160 °C for 20 h in an oven. The product obtained from autoclave was cooled at room temperature then washed several times in centrifuge machine with water and ethanol ultimately dried in oven about 60 °C for 7 h to get Fe₂O₃ nano rods.



Figure 2.2: Synthesis of Iron Oxide (Fe₂O₃) Nano rods

2.3. Synthesis of Carbon and Iron Oxide (C@Fe₂O₃) Nano rods:

To obtain Fe₂O₃@C, 0.01 g precursor was added in aqueous solution containing 10 ml ethanol and 5 ml distilled water by continue stirring in magnetic stirrer about 10 min. Then 0.1 gram glucose was added in solution after that the solution stirrer with the help of magnetic stirrer for 10 min. The resulting solution transferred to a 50 ml Teflon-lined stainless steel autoclave and heated at 120 °C for 16 h. The product obtained was cooled at room temperature then washed several times with water and ethanol by using centrifuge machine ultimately at 70 °C for about 9 h.

2.4. Synthesis of Nickel, Carbon and Iron Oxide (Ni@C@Fe₂O₃) Nano rods:

0.01 g Fe₂O₃ and 0.1 g Glucose were added in 20 ml ethanol and 5 ml H₂O solution stirred that solution for 10 minutes. Added 0.06 g Ni(NO₃)₂. 6H₂O in above solution and stirred for 15 minutes, placed that solution in autoclave and was heated at about 180 °C for 20 hour in an oven. After heating in oven centrifuge the solution and dry in oven at 70 °C for 6 h. Additionally, the sample was put into Ni boats with flowing nitrogen heated at 500 °C for 2 hour by using heating rate of about 5 °C per minute. The sample was then preserved for further characterization needs.

2.5. Characterization:

SEM and FT–IR were utilized to know the morphological and structural information of all of the synthesized samples. A QUANTA 450 (FEI, America) was used to take SEM images, which were united with energy dispersive spectroscopy (EDS) to observe the chemical constitution of samples. The structural features of porosity were investigated using N₂ adsorption desorption measurements. The distinct functional groups of samples were firm to use FT–IR spectroscopy lying on a Bruker–Tenson 27 in the 4000–400 cm⁻¹ range. The X-ray diffraction patterns were recorded at room temperature to use a Netherlands' PANalyticalX'pert power diffractometer with Cu K (=0.15408 nm) radiation to generate at 40 kV & 40 mA with a scan rate of 16° min⁻¹ utilizing Cu K (=0.15408 nm) radiation generated at 40 kV & 40 mA with a scan rate of 16° min⁻¹.

2.6. Electrochemical Tests:

A conventional three electrode cell was engaged for electrochemical capacity. The electrode for working was made as follows: as to synthesize samples, carbon blacks with binder (60% polytetrafluorethylene suspension in aqueous) were added at a mass ratio of 8:1:1 and was mixed thoroughly in N-methyl-2-pyrrolidone (NMP) in anticipation of a slurry with required viscosity was generated. Then slurry equivalently painted over a nickel foam like disk (with an active area of 1 cm²) by sinking, dried up at 80 °C for 12 hours in a vacuum drier oven, and pressure of 4 M Pa was applied for 30 seconds to make sure good electronic contact. So, working electrode was produced in this way. On a CHI 760e electrochemical terminal (CHENHUA, Shanghai, China), electrochemical capacity were measured.

3. Results and Discussion

3.1 Morphological and spectral properties:

SEM imaging technology is used to monitor the morphology of the formed sample. As to illustrate in Fig. 4.1 the Fe₂O₃, C@Fe₂O₃, and Ni@C@Fe₂O₃ samples have a distinct rod-like morphological structure with diameters of about 200 nm. It is obvious that nickel and carbon are both deposited over the surface of Fe₂O₃ nanorods to create Ni@C@Fe₂O₃ and C@Fe₂O₃, respectively.

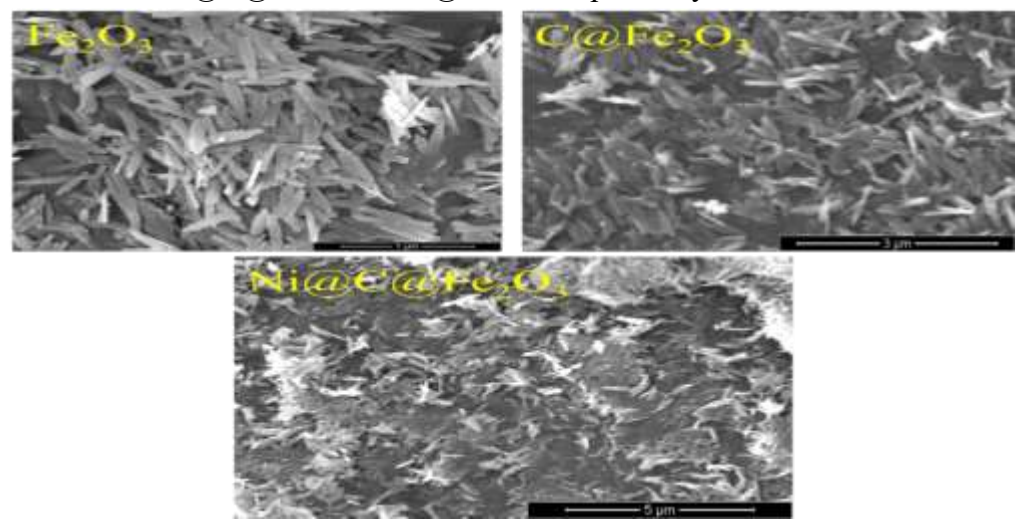


Figure 3.1: SEM images of different synthesized sample

To determine the elemental composition, EDS analysis is performed. The photos below display the obtained EDS results. Elemental analysis reveals the weight percentages of Fe (72.76%) and O (27.24%) corresponding to Fe₂O₃ nanorods, as seen in Fig. 3.2 (a). The elemental investigation in Fig. 4.2 (b) displays the weight percentage of Fe (26.89%), O (36.06%), and C (37.05%) corresponding to C@Fe₂O₃ nanorods. Over the surface and all through the middle of the Fe₂O₃ nanorods, C is shown to be scattered equally. The weight percentages of Fe (31.45%), O (35.60%), C (18.01%), and Ni (15.40%) corresponding to Ni@C@Fe₂O₃ nanorods are shown by elemental analysis in Fig. 4.2 (c). It demonstrates that the Ni and C components are evenly distributed across the whole Fe₂O₃ nanorod. The detected nano spheres are undoubtedly made of iron oxide since the Fe₂O₃ has a Fe/O weight percentage ratio of 3:4 and Ni@C@Fe₂O₃ has a Fe/O/C ratio of 3:4:3. Through EDX analysis, the elemental make up of the asprepared C@Fe₂O₃ and Ni@C@Fe₂O₃ is assessed. Fe and O of the as-prepared Fe₂O₃ nanorods are shown from the corresponding peaks in figure (3.2a). In accordance with Fe₂O₃ nanorods, the elemental composition of the nanorods shows 72.76% weight of iron and 27.24% weight of oxygen. Two distinct peaks can be seen in the EDX spectrum, one between 0 and 2 KeV and the other between 6 and 8 KeV, which corresponds to crystalline Fe₂O₃ nanorods.

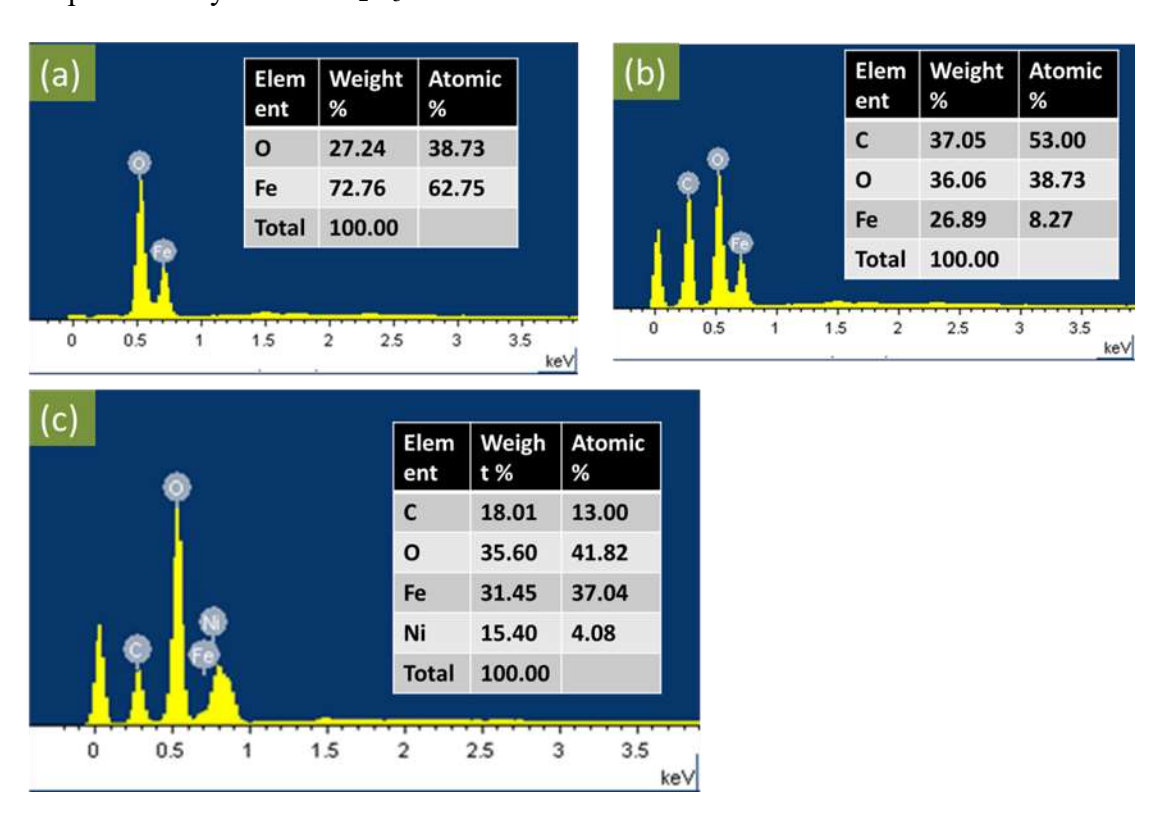


Figure 3.2: EDX of (a) Fe₂O₃, (b) C@Fe₂O₃ nano composite, (c) Ni@C@Fe₂O₃ nano composite

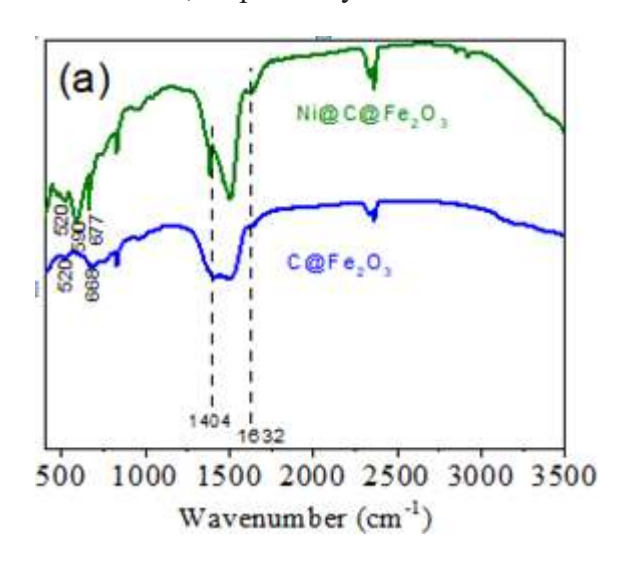
FT-IR study is utilized to resolve the various functional groups that are present in various samples of Fe₂O₃, C@Fe₂O₃, and Ni@C@Fe₂O₃ (Figure 4.3a). The presence of a major peak, for instance 520 cm⁻¹, it can be recognized that Fe and O in FTIR spectra demonstrated iron oxide was present in both as synthesized nano composite materials (116). Due to the occurrence of a significant peak at 668 cm⁻¹ that may be approved to carbon, iron and oxygen in FTIR spectra of C@Fe₂O₃ nano composite materials (121). Due to the occurrence of a significant peak in the FTIR spectrum at 590 cm⁻¹, which may be proved

to Ni, C, Fe and O present in Ni@C@Fe₂O₃ nano composite materials. Peaks at about 1600 cm⁻¹ and 1400 cm⁻¹ to cause by stretching vibrations of the O-H bond and C-O bond, respectively, formed by the hydroxyl groups over the surface of nano particles (117).

The phase structures of the samples were studied by powder X-ray diffraction (XRD). Fig.4.3(b), illustrates the XRD patterns of the C@Fe₂O₃, and Ni@C@Fe₂O₃, respectively. It clearly shows that all of these samples present a broad diffraction band at about 23.2°, which is related to amorphous structure of carbon. It confirms the presence of carbon in all metal oxides samples.

Fig.3.3(b), shows XRD pattern of as synthesized C@Fe₂O₃ exhibiting peaks at 2θ at 30.1°, 35.5°, 42.6°, 53.6°, 57.0° and 62.8° which can be assigned to diffraction of the (220), (331), (400), (422), (511), and (440) planes, respectively of spinal structured magnetite nano particles (118).

In Ni@C@Fe₂O₃ sample, diffraction peaks at 2θ values corresponding to 18.91° , 30.5° , 36° , 43.5° , 54° , 57.5° and 63° can be indexed to (111), (220), (311), (222), (400), (422), (511) and (440) crystal planes of Ni and Fe₂O₃, respectively.



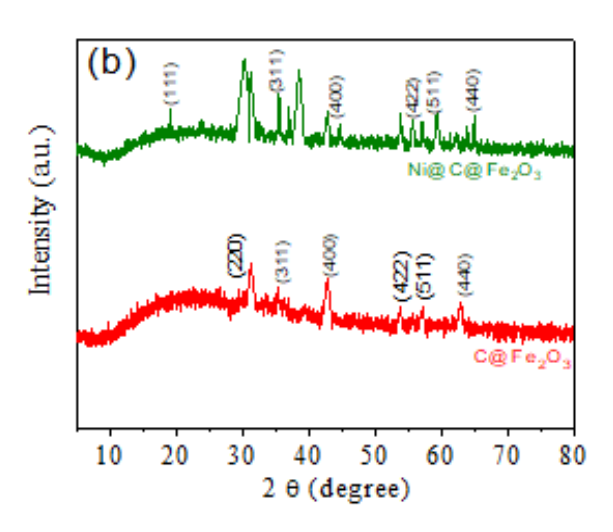


Figure 3.3: (a) Spectrum of FTIR of C@Fe₂O₃ and Ni@C@Fe₂O₃ (b) Xrd of C@Fe₂O₃ and Ni@C@Fe₂O₃

3.2 Electrochemical performance of C@Fe₂O₃ and Ni@C@Fe₂O₃

By using of cyclic voltammetry (CV), galvano static charge discharge (GCD), cyclic-stability, and electrochemical impedance spectroscopy, the electrochemical character of C@Fe₂O₃ and Ni@C@Fe₂O₃ samples are examined. At potentials range from 1.5 to -0.5 V versus Ag/AgCl and at different scan speeds range from 2 to 100 mVs⁻¹, cyclic voltammograms (CVs) were captured in 1.0 M KOH solution. As seen in Fig. 4.4(A), the curve of CV exhibits a nonrectangular shape, demonstrating the pseudo capacitance characteristics of the C@Fe₂O₃. Additionally, when rate of the scan increase, these CV shape curves essentially remains same, showing a rapid redox reaction and easy to access for ions to the electrode electrolyte boundary, favouring marvelous capacitance and electrochemical performance at low resistance. The fast redox reaction and ion transport are thought to be aided by the excellent dispersion

and well oriented structure of the $C@Fe_2O_3$ nanocomposites. The $C@Fe_2O_3$ CV curves in Fig. 3.4(A) clearly suggested that it had two redox peaks and a typical pseudo capacitive nature. Scan rate is seen against specific capacitance within Figure 3.4(C).

The equation is used to calculate the Cs values from CV curves.

$$S_{area} = \int IdV = \int Ivdt = v \int Idt = 2vQ \tag{1}$$

$$C_{z} = \frac{\Delta Q}{\Delta V(X)} = \frac{\int I dV}{2v(X)\Delta V} = \frac{S_{area}}{2v(X)\Delta V}$$
(2)

In this case, IdV stand for the potential window (V), mass of the samples (X), scan rate (Vs⁻¹), and incorporated area of the CV curve. At the scan speed of 2 to 100 mVs⁻¹, the Cs values of the nanocomposites C@Fe₂O₃ and Ni@C@Fe₂O₃ are displayed in Fig. 3.4 (A,B). The steady decrease in capacitive behavior of the samples is seen in Fig. 3.4 (C) when scan rate is amplified. At low scan rates, electrolyte ions strongly utilize both the exterior and interior surface pores of the active material, increasing the material's specific capacity. At high scan rates, the available active material's surface to electrolyte (OH⁻) ions is constrained (just the external regions of the holes). C@Fe₂O₃ shows Cs values of 870 Fg⁻¹, and at a scan rate about 2 mVs⁻¹, Ni@C@Fe₂O₃ nanorods exhibit the largest specific capacitance (1360 Fg⁻¹). This is thought to be due to their high SSA.

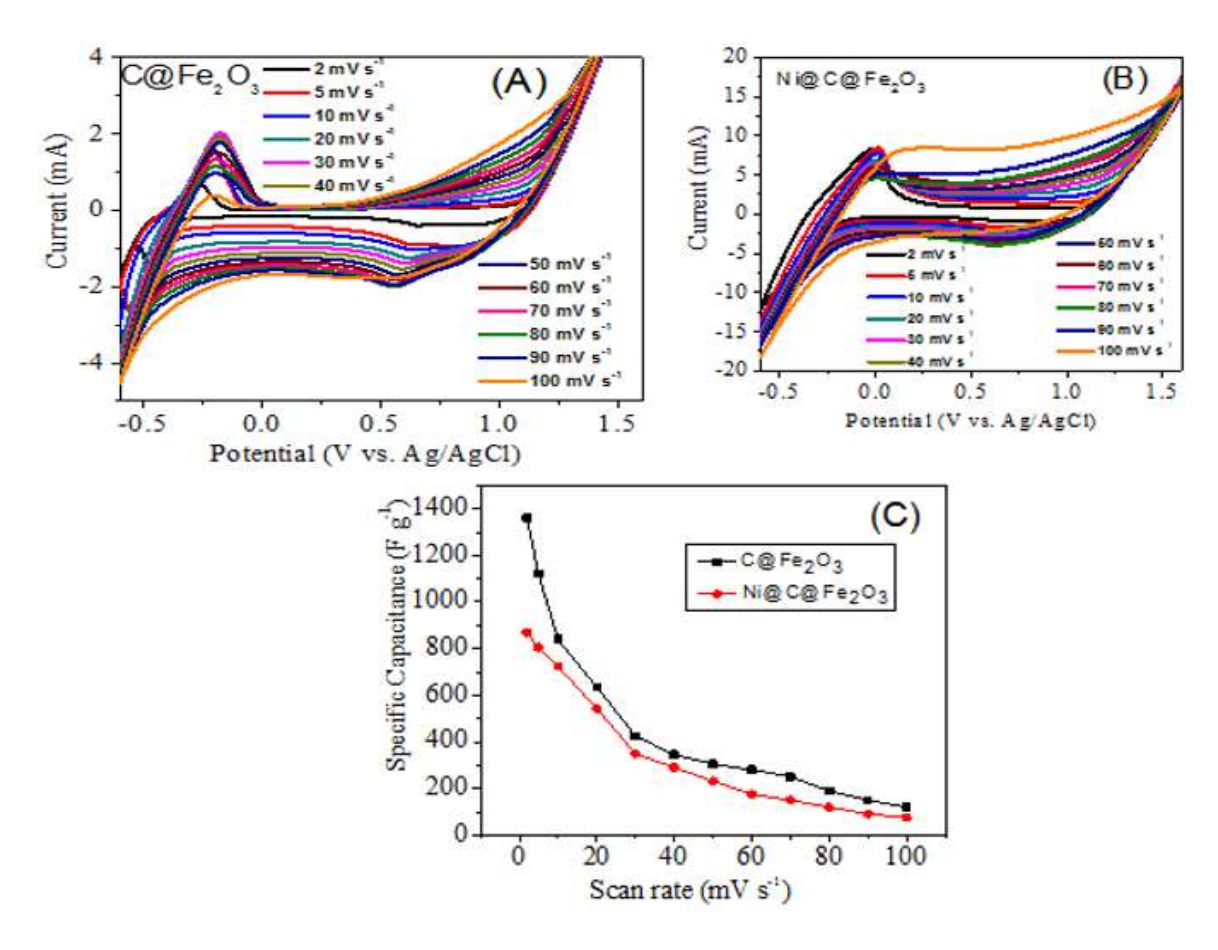
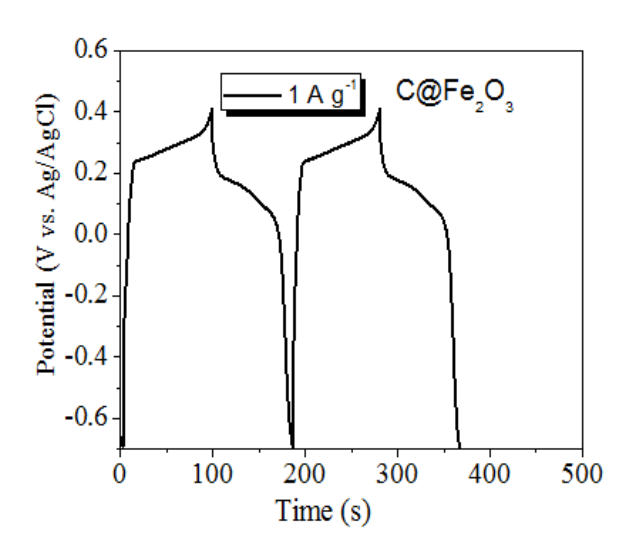


Figure 3.4: (A) CV curve of C@Fe₂O₃ (B) CV curve of Ni@C@Fe₂O₃

(C) Specific capacitance vs scan rate

In 1.0 M KOH electrolyte at 1 and 5 Ag⁻¹ current density contained by the potential window of -0.6 to 0.6 V against Ag/AgCl, GCD curves of C@Fe₂O₃ and Ni@C@Fe₂O₃ nanocomposites samples were conducted (figure 4.5, 4.6, 4.7, 4.8). As illustrated in Fig. 4.5, 4.6, 4.7, and 4.8 discharge patterns of electrodes are not usual straight lines but fairly curved, demonstrating the pseudo capacitive characteristics of C@Fe₂O₃ and the prolonged discharge times of Ni@C@Fe₂O₃ nanocomposites, which display high specific capacitance.

C@Fe₂O₃ has a cyclic stability of 70% withholding over 1500 cycles, whereas Ni@C@Fe₂O₃ nanorods have a cyclic stability of 85% retention over 1500 cycles, which is much privileged than that of C@Fe₂O₃ nanorods (Figure 3.9. a).



0.4 5 A g⁻¹ Potential (V vs. Ag/AgCI) 0.2 C@Fe₂O₃ 0.0 0.2-0.4-0.6 50 100 150 200 250 300 Time (s)

Figure 3.5: GCD curve of $C(a)Fe_2O_3$

0.4 1 A g⁻¹ Potential (V vs. Ag/AgCl) 0.2 0.0 -0.2 Vi@C@Fe¸C -0.4 -0.6 600 200 400 800 Time (s)

Potential (V vs. Ag/AgCI) -0.2-0.4-0.6 200 400 600 Time (s)

Figure 3.7: GCD curve of Ni@C@Fe₂O₃

Figure 3.8: GCD curve of Ni@C@Fe₂O₃

Figure 3.6: GCD curve of C@Fe₂O₃

5 Ag

C@Ni@Fe,O,

0.4

0.2

0.0

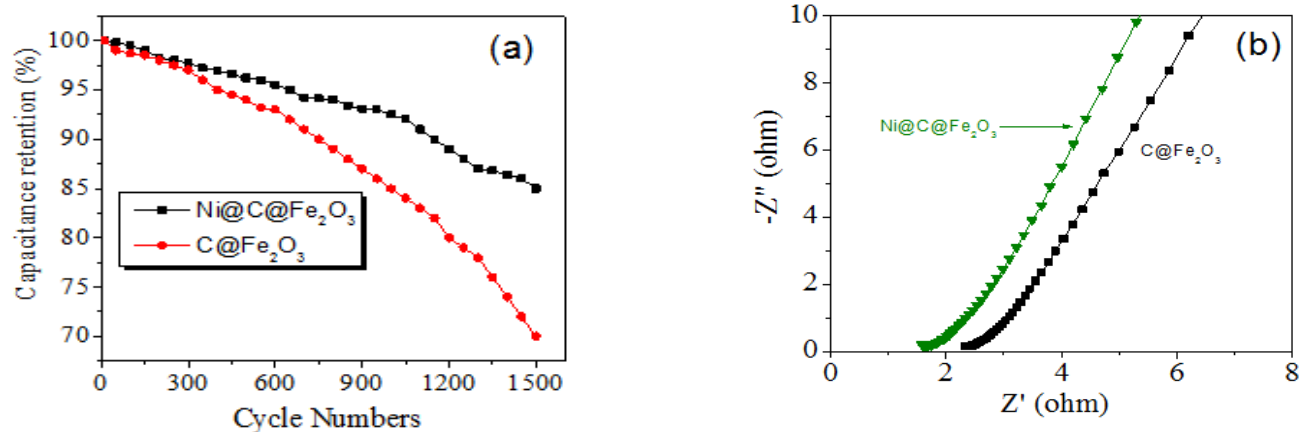


Figure 3.9: (a) Cyclic stability of C@Fe₂O₃ and Ni@C@Fe₂O₃ (b) EIS graph of C@Fe₂O₃ and Ni@C@Fe₂O₃

Electrochemical impedance spectroscopy (EIS) is a method for measuring the character of any substance's conductivity as a task of frequency. Data collected from the EIS may be expressed to use the Nyquist plot. The Nyquist plot compare the pretend impedance constituent (Z') to the real impedance component (Z''). The higher frequency intercept of the actual component of impedance is what to determine the solution resistance (Rs) of the composite. In the upper frequency range, a depressed semicircular is employed to show the charge transfer resistance (Rs) that is predominantly produced by the charge transfer process of the electrode materials. The $C@Fe_2O_3$ sample has a short solution resistance and charge transfer. The lowest Rs value for $Ni@C@Fe_2O_3$ nanorods, however, is attributed to substantial electrical conductivity. In comparison to $C@Fe_2O_3$ nanorods, $Ni@C@Fe_2O_3$ nanorods have a smaller semicircle diameter, which suggests high conductivity. Fig. 3.9 (b) shows that the activated $Ni@C@Fe_2O_3$ nanorods exhibit good electronic conductivity and a low Rs for charge transfer. $Ni@C@Fe_2O_3$ nanorods have a straighter profile than $C@Fe_2O_3$ nanorods at low frequencies. This demonstrates the superior specific capacitance and low ion diffusion resistance of $Ni@C@Fe_2O_3$ nanorods. $Ni@C@Fe_2O_3$ nanorods have shown to be ideal for usage in super capacitor type applications with high electrochemical characteristics due to their comparably reduced resistance.

Conclusion

There will inevitably be an energy crisis because of the rising usage of energy equipment brought on by rapid economic and population expansion. The public's interest in research on renewable energy and energy efficiency has increased as a result. Society must transition to clean and renewable energy sources while simultaneously managing resource use. High electrochemical characteristics, including high porosity, low rate, efficient capacitance, and a variety of morphologies, including nano wires, nanorods, nano walls, nano flowers, and nano sheets, are displayed by Ni@C@Fe₂O₃ based nanocomposites. In this study, we used the conventional hydrothermal approach to create Ni@C@Fe₂O₃ based nanocomposites employing cost effective ingredients such as urea, ferric chloride hexahydrate, potassium hydroxide, glucose, and nickel nitrate hexahydrate. Urea, ferric chloride hexahydrate, and potassium hydroxide are used to make Fe₂O₃ nanorods. To create a composite of C@Fe₂O₃ nanorods, carbon is deposited on top of the as prepared Fe₂O₃ nanorods, which are employed as templates. Then, to create Ni@C@Fe₂O₃ nanorods composite, the as prepared Fe₂O₃ nanorods are employed as templates and carbon with nickel is

deposited over the Fe_2O_3 nanorods. Fe_2O_3 , $C@Fe_2O_3$, and $Ni@C@Fe_2O_3$ nanorods as synthesized are structurally determined using SEM, XRD, EDS, and FT-IR.

Through CV, Cyclic Stability, GCD curve measurements, and EIS, the electrochemical characteristics of nanocomposites have been examined. 1.0 M KOH aqueous solution of Ni@C@Fe₂O₃ nanorods showed elevated specific-capacitance of about 840 Fg⁻¹ with a scan rate of 10 mVs⁻¹ and capacitance-retention 85% over about 1500 cycles. From all of these findings, it can be deduced that nanocomposites made of C@Fe₂O₃ and Ni@C@Fe₂O₃ perform extremely well electrochemically. Ni@C@Fe₂O₃ nanocomposites can have their electrochemical characteristics further enhanced by heated at high temperatures, such as 500 °C for 2 h.

REFERENCES

1. Bagarti T, Jayannavar AM. Storage of electrical energy. Resonance. 2020;25(7):963-80.

- **2.** Catenaro E, Rizzo DM, Onori S. Experimental analysis and analytical modeling of enhanced-Ragone plot. Applied Energy. 2021;291:116473.
- **3.** Goetz JL, Keltner D, Simon-Thomas E. Compassion: an evolutionary analysis and empirical review. Psychological bulletin. 2010;136(3):351.
- **4.** Qing H, Li Z, Yang Z, Shi M, Huang Z, Song J, et al. The possibility of COVID-19 transmission from eye to nose. Acta ophthalmologica. 2020.
- 5. Wei Z-X, Zhu Y-T, Liu J-Y, Zhang Z-C, Hu W-P, Xu H, et al. Recent advance in single-atom catalysis. Rare Metals. 2021;40(4):767-89.
- 6. Barros AJ, Ronsmans C, Axelson H, Loaiza E, Bertoldi AD, França GV, et al. Equity in maternal, newborn, and child health interventions in Countdown to 2015: a retrospective review of survey data from 54 countries. The Lancet. 2012;379(9822):1225-33.
- 7. Bryan ML, Knutson HA, Howard AW, Ngo H, Batygin K, Crepp JR, et al. Statistics of long period gas giant planets in known planetary systems. The Astrophysical Journal. 2016;821(2):89.
- **8.** Taamalli A, Feriani A, Lozano-Sanchez J, Ghazouani L, El Mufti A, Allagui MS, et al. Potential hepatoprotective activity of super critical carbon dioxide olive leaf extracts against CCl4-induced liver damage. Foods. 2020;9(6):804.
- 9. Demetri GD, Von Mehren M, Antonescu CR, DeMatteo RP, Ganjoo KN, Maki RG, et al. NCCN Task Force report: update on the management of patients with gastrointestinal stromal tumors. Journal of the National Comprehensive Cancer Network. 2010;8(Suppl_2):S-1-S-41.
- **10.** Arzoumanian Z, Baker PT, Blumer H, Bécsy B, Brazier A, Brook PR, et al. The NANOGrav 12.5 yr data set: search for an isotropic stochastic gravitational-wave background. The Astrophysical journal letters. 2020;905(2):L34.
- 11. Gupta AK, Smith KG, Shalley CE. The interplay between exploration and exploitation. Academy of management journal. 2006;49(4):693-706.
- **12.** Pavlov VA, Chavan SS, Tracey KJ. Molecular and functional neuroscience in immunity. Annual review of immunology. 2018;36:783.
- **13.** Bikbov B, Purcell CA, Levey AS, Smith M, Abdoli A, Abebe M, et al. Global, regional, and national burden of chronic kidney disease, 1990–2017: a systematic analysis for the Global Burden of Disease Study 2017. The lancet. 2020;395(10225):709-33.
- 14. Xiangyu X, Ye W, Zhang S, Wang Q, Jiang H, Wu W, editors. Capturing event argument interaction via a bi-directional entity-level recurrent decoder. Proceedings of the 59th Annual Meeting of the

Association for Computational Linguistics and the 11th International Joint Conference on Natural Language Processing (Volume 1: Long Papers); 2021.

- **15.** Tacconelli E, Carrara E, Savoldi A, Harbarth S, Mendelson M, Monnet DL, et al. Discovery, research, and development of new antibiotics: the WHO priority list of antibiotic-resistant bacteria and tuberculosis. The Lancet Infectious Diseases. 2018;18(3):318-27.
- **16.** Hirsch JS, Ng JH, Ross DW, Sharma P, Shah HH, Barnett RL, et al. Acute kidney injury in patients hospitalized with COVID-19. Kidney international. 2020;98(1):209-18.
- 17. Liu D, Zhang W, Lin H, Li Y, Lu H, Wang Y. A green technology for the preparation of high capacitance rice husk-based activated carbon. Journal of cleaner production. 2016;112:1190-8.
- **18.** Dubal DP, Ayyad O, Ruiz V, Gomez-Romero P. Hybrid energy storage: the merging of battery and supercapacitor chemistries. Chemical Society Reviews. 2015;44(7):1777-90.
- 19. Choi NS, Chen Z, Freunberger SA, Ji X, Sun YK, Amine K, et al. Challenges facing lithium batteries and electrical double-layer capacitors. Angewandte Chemie International Edition. 2012;51(40):9994-10024.
- 20. Shi H. Activated carbons and double layer capacitance. Electrochimica Acta. 1996;41(10):1633-9.
- 21. Salitra G, Soffer A, Eliad L, Cohen Y, Aurbach D. Carbon electrodes for double-layer capacitors I. Relations between ion and pore dimensions. Journal of the Electrochemical Society. 2000;147(7):2486.
- **22.** Zhang LL, Zhao X. Carbon-based materials as supercapacitor electrodes. Chemical Society Reviews. 2009;38(9):2520-31.
- 23. Frackowiak E, Metenier K, Bertagna V, Beguin F. Supercapacitor electrodes from multiwalled carbon nanotubes. Applied Physics Letters. 2000;77(15):2421-3.
- **24.** Cheng Q, Tang J, Ma J, Zhang H, Shinya N, Qin L-C. Graphene and carbon nanotube composite electrodes for supercapacitors with ultra-high energy density. Physical Chemistry Chemical Physics. 2011;13(39):17615-24.
- 25. Du C, Yeh J, Pan N. High power density supercapacitors using locally aligned carbon nanotube electrodes. Nanotechnology. 2005;16(4):350.
- **26.** Rui S, Lu J, Chunxu P. A single-step process for preparing supercapacitor electrodes from carbon nanotubes. Soft Nanoscience Letters. 2011;2011.
- 27. Syarif N, Tribidasari A, Wibowo W. Direct synthesis carbon/Metal oxide composites for electrochemical capacitors electrode. Int Trans J Eng Manag Appl Sci Technol. 2012;3:21-34.
- **28.** Frackowiak E, Beguin F. Carbon materials for the electrochemical storage of energy in capacitors. Carbon. 2001;39(6):937-50.

29. Arbizzani C, Mastragostino M, Soavi F. New trends in electrochemical supercapacitors. Journal of power sources. 2001;100(1-2):164-70.

- **30.** Moreno-Fernandez G, Ibañez J, Rojo JM, Kunowsky M. Activated carbon fiber monoliths as supercapacitor electrodes. Advances in Materials Science and Engineering. 2017;2017.
- **31.** Pandolfo AG, Hollenkamp AF. Carbon properties and their role in supercapacitors. Journal of power sources. 2006;157(1):11-27.
- 32. Salunkhe RR, Lin J, Malgras V, Dou SX, Kim JH, Yamauchi Y. Large-scale synthesis of coaxial carbon nanotube/Ni (OH) 2 composites for asymmetric supercapacitor application. Nano Energy. 2015;11:211-8.
- **33.** Simon P, Burke A. Nanostructured carbons: double-layer capacitance and more. The electrochemical society interface. 2008;17(1):38.
- **34.** Pan H, Li J, Feng Y. Carbon nanotubes for supercapacitor. Nanoscale research letters. 2010;5(3):654-68.
- **35.** Raymundo-Pinero E, Kierzek K, Machnikowski J, Béguin F. Relationship between the nanoporous texture of activated carbons and their capacitance properties in different electrolytes. Carbon. 2006;44(12):2498-507.
- **36.** Arenillas A, Menéndez JA, Reichenauer G, Celzard A, Fierro V, Hodar FJM, et al. Organic and Carbon Gels: From Laboratory Synthesis to Applications: Springer; 2019.
- 37. Alam SN, Sharma N, Kumar L. Synthesis of graphene oxide (GO) by modified hummers method and its thermal reduction to obtain reduced graphene oxide (rGO). Graphene. 2017;6(1):1-18.
- **38.** Tan YB, Lee J-M. Graphene for supercapacitor applications. Journal of Materials Chemistry A. 2013;1(47):14814-43.
- **39.** Liu C, Yu Z, Neff D, Zhamu A, Jang BZ. Graphene-based supercapacitor with an ultrahigh energy density. Nano letters. 2010;10(12):4863-8.
- **40.** Wang H, Hao Q, Yang X, Lu L, Wang X. A nanostructured graphene/polyaniline hybrid material for supercapacitors. Nanoscale. 2010;2(10):2164-70.
- **41.** Pumera M. Graphene-based nanomaterials and their electrochemistry. Chemical Society Reviews. 2010;39(11):4146-57.
- **42.** Karthika P, Rajalakshmi N, Dhathathreyan KS. Functionalized exfoliated graphene oxide as supercapacitor electrodes. 2012.
- **43.** Kim T, Jung G, Yoo S, Suh KS, Ruoff RS. Activated graphene-based carbons as supercapacitor electrodes with macro-and mesopores. ACS nano. 2013;7(8):6899-905.

44. Sinniah GK, Shah MZ, Siong HC, editors. The needs for changes in travel behaviour towards a Low Carbon Society. Proceedings of the 26th International Business Information Management Association Conference—Innovation Management and Sustainable Economic Competitive Advantage: From Regional Development to Global Growth, IBIMA; 2015.

- **45.** Chen S-M, Ramachandran R, Mani V, Saraswathi R. Recent advancements in electrode materials for the high-performance electrochemical supercapacitors: a review. Int J Electrochem Sci. 2014;9(8):4072-85.
- **46.** Wang Y, Shi Z, Huang Y, Ma Y, Wang C, Chen M, et al. Supercapacitor devices based on graphene materials. The Journal of Physical Chemistry C. 2009;113(30):13103-7.
- 47. Zhang LL, Zhao X, Stoller MD, Zhu Y, Ji H, Murali S, et al. Highly conductive and porous activated reduced graphene oxide films for high-power supercapacitors. Nano letters. 2012;12(4):1806-12.
- **48.** Paek E, Pak AJ, Kweon KE, Hwang GS. On the origin of the enhanced supercapacitor performance of nitrogen-doped graphene. The Journal of Physical Chemistry C. 2013;117(11):5610-6.
- **49.** Palaniselvam T, Kashyap V, Bhange SN, Baek JB, Kurungot S. Nanoporous graphene enriched with Fe/Co-N active sites as a promising oxygen reduction electrocatalyst for anion exchange membrane fuel cells. Advanced Functional Materials. 2016;26(13):2150-62.
- **50.** Li N, Tang S, Dai Y, Meng X. The synthesis of graphene oxide nanostructures for supercapacitors: a simple route. Journal of Materials Science. 2014;49(7):2802-9.
- **51.** Cheng Q, Tang J, Shinya N, Qin L-C. Polyaniline modified graphene and carbon nanotube composite electrode for asymmetric supercapacitors of high energy density. Journal of Power Sources. 2013;241:423-8.
- **52.** Han G, Liu Y, Zhang L, Kan E, Zhang S, Tang J, et al. MnO2 nanorods intercalating graphene oxide/polyaniline ternary composites for robust high-performance supercapacitors. Scientific reports. 2014;4(1):1-7.
- **53.** Li J, Xie H, Li Y, Liu J, Li Z. Electrochemical properties of graphene nanosheets/polyaniline nanofibers composites as electrode for supercapacitors. Journal of Power Sources. 2011;196(24):10775-81.
- **54.** Snook GA, Kao P, Best AS. Conducting-polymer-based supercapacitor devices and electrodes. Journal of power sources. 2011;196(1):1-12.
- **55.** Wang K, Huang J, Wei Z. Conducting polyaniline nanowire arrays for high performance supercapacitors. The Journal of Physical Chemistry C. 2010;114(17):8062-7.
- **56.** Zhou C, Zhang Y, Li Y, Liu J. Construction of high-capacitance 3D CoO@ polypyrrole nanowire array electrode for aqueous asymmetric supercapacitor. Nano letters. 2013;13(5):2078-85.